Nano Hybrids *Online: 2012-08-22*
ISSN: 2234-9871, Vol. 2, pp 65-85
doi:10.4028/www.scientific.net/NH.2.65

Nanocomposites of Carbonated Hydroxyapatite/Poly(4-vinyl pyridine-co-Styrene): Synthesis, Characterization and its Application

C.P. Dhanalakshmi[1], L. Vijayalakshmi[2] and V. Narayanan[1]*

[1]Department of Inorganic Chemistry, University of Madras, Guindy Campus, Chennai –600 025, Tamil Nadu, India.

[2]Department of chemistry, S.D.N.B. Vaishnav college for women, Chrompet, Chennai-600044, Tamil Nadu, India.

*Address for Correspondence: Email: vnnara@yahoo.co.in, Phone: +91 44 22202793; Fax: +91 44 22300488.

Keywords: Carbonated hydroxyapatite, nanocrystalline, nanocomposite, Poly(4-vinyl pyridine-co-styrene)

Abstract. Nano carbonated hydroxyapatite/Poly(4-vinyl pyridine-co-styrene) composites of varying composition for biomaterial applications have been synthesized. The nano carbonated hydroxyapatite/Poly(4-vinyl pyridine-co-styrene) composite materials were characterized by XRD, FTIR, ^{31}P NMR, TGA, DTA and FESEM. Carbonated Hydroxyapatite nano rod embedded composite was prepared using Poly(4-vinyl pyridine-co-styrene) as a matrix with different weight percentages (wt %). The results indicated that the size and crystallinity of Carbonated hydroxyapatite nano particles decreases with increase in Poly(4-vinyl pyridine-co-styrene) concentration in the composite. SEM confirms the presence of carbonated hydroxyapatite nano rod crystals in Poly(4-vinyl pyridine-co-styrene) matrix. Nano Carbonated hydroxyapatite/ Poly(4-vinyl pyridine-co-styrene) composites were screened for antimicrobial activity and anti inflammatory activity.

Introduction

The mineral phase of hard tissue is a so-called biological apatite, i.e. a non-stoichiometric hydroxyapatite. Pure hydroxyapatite has the formula $Ca_{10}(PO_4)_6(OH)_2$. In contrast, a biological apatite (like in bone) is non-stoichiometric and contains several other ions, mainly carbonate (some percent) and other elements in traces like Mg^{2+}, Na^{+}, Fe^{2+}, HPO_4^{2-}, F^{-}, Cl^{-}. Consequently, a more appropriate structural formula for the composition of bone is $(Ca, X)_{10}(PO_4, CO_3, Y)_6(OH, Z)_2$ with X substituting cations and Y and Z substituting anions (with the indices 10, 6 and 2 changing according to stoichiometry) [1–5]. Despite numerous attempts, there is still a strong need for synthetic bone substitution materials in clinical applications. Synthetic bone substitution materials comprise biologically derived materials (e.g. collagen), inorganic materials (e.g. calcium phosphates or bioglass), organic materials (e.g. biodegradable polyesters) and composite materials (mixtures and compositions of the above-mentioned categories) [6]. Due to their excellent biocompatibility, a multitude of calcium phosphate biomaterials is available for clinical treatment of bone defects [2, 3]. The most prominent examples are calcium phosphates of high crystallinity (e.g. from calcined bovine spongiosa) [7], nano apatites from chemical precipitation [8,9], and bone cements that harden in the defect [10]. Especially in the first case, a lack of resorption rate has been reported [7] that can be ascribed to a low solubility of these materials under physiological conditions of osteoclastic bone resorption (i.e. at a pH between 4 and 5) [11–13]. In contrast, bone mineral consists of nano crystals that have a higher solubility due to thermodynamic reasons [14]. Additionally, all biological apatites contain a few percent of carbonate ions that occupy phosphate and possibly hydroxide positions [15]. This leads to structural disorder and also to a higher solubility [16]. An optimised biomaterial should therefore be as biomimetic as possible,i.e. consist of poorly crystalline, carbonate substituted apatite that, however, can still be processed into objects with a sufficient mechanical stability. Generally, the composite biomaterials are prepared by using biocompatible/biodegradable and synthetic/natural polymers [17,18].

The inorganic minerals such as hydroxyapatite [19], bioactive glasses [20], metal oxides [21], and carbon nanotube [22] are incorporated into polymer matrixes to impart bioactivity. This enables us to develop the composite with desired properties [23,24].

The addition of nano sized particles is desirable to develop the composite with a good mechanical strength since the natural bone contains mineral crystals which are at the nanometer scale and embedded in the collagen matrix [25]. The polymer composites are designed to meet the specific requirement of biomedical applications like tissue engineering and drug delivery system. The right choice of the composition of both filler and polymer matrix are essential in addition to the process method to obtain suitable biopolymer composites. Recently, attempts have been made to develop nano composites, wherein nano carbonated hydroxyapatite particles are embedded in PVPCS(Poly(4-vinyl pyridine-co-styrene)) polymeric matrices [25-27].

An extensive study have been made on both natural (collagen, gelatin, silk fibroin) and synthetic (polyethylene, polyamide, chitosan, polystyrene, poly(vinyl alcohol) and poly(etheretherketone)) polymers to overcome the mechanical problems associated with bio ceramics in bone tissue engineering applications [28-31]. Among the above polymers, Poly(4-vinyl pyridine-co-styrene) remain one of the widely used polymer group of biomaterials applied for medical implants. This usage is due to its segmented block co-polymer character. This wide range of versatility is utilized in terms of tailoring their applications such as tissue scaffolding [32], artificial cartilage [33] and biodegradable scaffolds [34]. In this paper nao CHAp/PVPCS nano composite is prepared and characterzed. This biomaterial will be easy to adhere to tissue and fix in site for a long-term. This composite is a very promising material for use in artificial articular cartilage.

Experimental

Materials. Analytical grade calcium nitrate ($Ca(NO_3)_2$), Poly(ethylene glycol) (PEG)and diammonium dihydrogen phosphate ($(NH_4)_2HPO_4$) were obtained from Merck (India). Poly(4-vinyl pyridine-co-styrene) was purchased from Loba and used as received. Doubly distilled water was used as the solvent.

Synthesis of nano Carbonated Hydroxyapatite. The nano CHAp was synthesized by following a modified wet chemical method. $Ca(NO_3)_2$ and the PEG were dissolved in a 50 ml distilled water to form a $Ca(NO_3)_2$ solution with a PEG:Ca^{2+} weight ratio of 4:1. $(NH_4)_2HPO_4$ and $(NH_4)_2CO_3$ were first dissolved in 50 ml distilled water to form a clear 0.10 M phosphate solution with an molar ratio of CO_3/PO_4 of 1:1 and then added dropwise to the PEG-$Ca(NO_3)_2$ solution with an initial Ca/P molar ratio of 1.60; the precipitation reaction was maintained at 5 °C under vigorous stirring for 30 min.The powdered samples of CHAp was obtained after heat treating the precipitate 800 °C for 3 h in a furnace (in air).

Synthesis of nano CHAp/PVPCS composites. The nano carbonated hydroxyapatite/PVPCS composites were coded as nano CHAp/PVPCS10 to nano CHAp/ PVPCS100, where nano carbonated hydroxyapatite denoted as nano CHAp and Poly(4-vinyl pyridine-co-styrene) denoted as PVPCS and the numbers denoted PVPCS wt%. Water was used as the solvent to prepare polymer solution. PVPCS was dissolved by using magnetic stirrer for 3 h and the polymer solution was left overnight in room temperature to remove the air bubbles trapped in the viscous solution. Then required amount of nano carbonated hydroxyapatite was dispersed in deionised water by 30 min ultrasonication. Ultrasonication was necessary to avoid agglomeration of ceramic powder and to achieve proper dispersion. Hydroxyapatite in water was mixed with polymer solution under agitation. The homogeneously mixed solution was taken into deep freeze at –18 °C and after 48 h of freezing the samples were freeze dried.

Physical Measurements. The prepared samples were studied by FTIR spectroscopy using a Schimadzu FT-IR 300 series instrument. The FTIR spectra were obtained over the region 450–4000 cm^{-1} in pellet form for 1 mg powder samples mixed with 200 mg spectroscopic grade KBr. Spectra were recorded at 4 cm^{-1} resolution averaging 80 scans. The structure of the samples were analyzed by a Rich Siefert 3000 diffractometer with Cu-Kα_1 radiation (λ = 1.5418 Å). The diffraction peak at 25.9° was chosen for calculation of the crystallite size by Scherrer formula since it is sharper and isolated from others. This peak assigns to (002) Miller's plane family and shows the crystal growth along the axis of carbonated HAp crystalline structure. The morphology of the materials was analyzed by FESEM using a HITACHI S600N scanning electron microscopy. For the elemental analysis the electron microscope was equipped with an energy dispersive X-ray attachment. Thermo gravimetric analysis (TGA) coupled with differential thermal analysis (DTA) of the material was performed (STA 1500, PL Thermal Science) between 35 °C and 1400 °C in air at a heating rate of 20 K per minute to monitor the weight loss of organic residues.

Anti –inflammatory activity test by HRBC membrane stabilization method. The human red blood cells (HRBC) membrane stabilization has been used as method to study the anti-inflammatory activity. After approbation of Human Research Ethics Committee and signed consent form, blood samples collected from healthy volunteer were used in this test. The harvest blood was mixed with equal volume of sterilised Alsever solution (2% dextrose, 0.8% sodium citrate, 0.05% citric acid and 0.42% sodium chloride in water). The blood was centrifuged at 3000 rpm and packed cell were washed with isosaline (0.85%, pH 7.2) and a 10% (v/v) suspension was made with isosaline. The assay mixture contained the drug (various concentrations g/ml), 1 ml of phosphate buffer (0.15M,pH 7.4), 2 ml of hyposaline (0.36%) and 0.5 ml of HRBC suspension. Diclofenac (Sigma Aldrich,India) was used as reference drug. Instead of hyposaline 2 ml of distilled water was used in the control. All the assay mixture were incubated at 37 °C for 30 min and centrifuged. The hemoglobin content in the supernatant solution was estimated using spectrophotometer at 560 nm (Shimadzu Scientific

Instruments,USA). The percentage protection was calculated by assuming the hemolysis produced in presence of distilled water of as 100%. The percentage of haemolysis was calculated using the formula:

$$\% \text{ Protection} = \frac{100 \text{ --- Optical density of drug treated sample}}{\text{Optical density of control}} \times 100$$

Preparation of the modified electrode. Ultrasonic agitation for 30 min was used to disperse 1 mg of thesynthesized nanoparticles into 5 ml of acetone to make homogeneous suspension. The highly polished GCE was coated with 5µL of the above suspension and dried in air.The modified electrode was activated in 0.1 M KCl solution by successive cyclic scans between -0.1 and +0.6 V . Before and after each experiment,the modified electrode was washed with distilled water and reactivated by the method mentioned above.

Results and Discussion

XRD Analysis. The XRD patterns of nano CHAp and nano CHAp/ PVPCS composites were taken. The patterns indicate the presence of amorphous CHAp. The broad peaks reveal that the particles sizes are very small in the range of 30 to 70 nm. The reflection planes corresponding to the characteristic XRD spectral peaks of pure nano CHAp and PVPCS/CHAp nanocomposites are shown in Fig. 1. The observed diffraction peaks are identified by standard JCPDS file (no. 35-0180) and are assigned as crystalline CHAp. The XRD patterns show diffraction peaks with line broadening and high intensities, which confirms the nanosize with crystalline nature. The diffraction peaks particularly in the planes (002), (211), (112) and (300) are high and narrow implying that the

CHAp crystallizes well. The crystallite size of the pure CHAp and PVPCS/CHAp composite is calculated by using Scherrer's formula [35]. Fig. 1 reveals that the crystallite size decreases with increase in the composition of PVPCS [36].

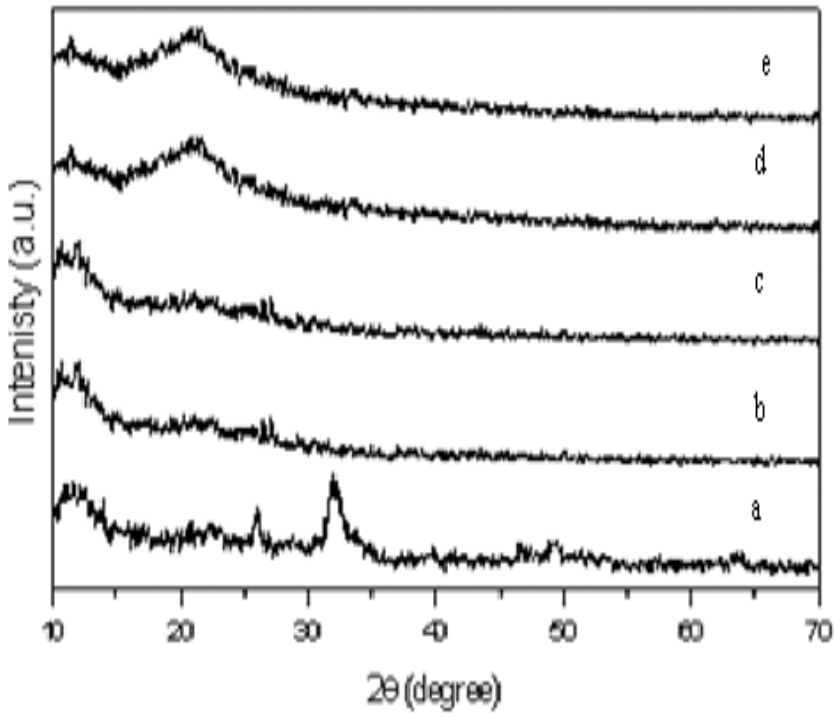

Fig. 1. XRD Pattern of (a) nano CHAp, (b) nano CHAp/PVPCS 20, (c) nano CHAP/PVPCS 40, (d) nano CHAp/PVPCS 60 and (e) nano CHAp/PVPCS 80.

FTIR Analysis. The FTIR spectra of pure nano CHAp and nano PVPCS/CHAp composites are shown in Fig. 2. The ν_2 phosphate stretching mode is appeared at 459-480 cm^{-1} corresponds to PO_4^{3-} group in CHAp. The bands located at 1030-1060 and 526-567 cm^{-1} are attributed respectively to the ν_3 and ν_4 P-O vibration modes of regular tetrahedral PO_4^{3-} groups . The observed bands at 602 cm^{-1} corresponds to O-P-O bending and ν_1 symmetric P-O stretching modes. The ν_1 symmetric stretching mode of phosphate group is observed at 962 cm^{-1}. The observed bands at 1418 cm^{-1} is due to the stretching mode of carbonate, which may be due to the acquisition of air during mineral

precipitation. Similarly, the observed bands at 1416-1419 and 824-873 cm^{-1} are assigned to carbonate ions. The lattice H_2O exists in the range of 1601-1638 cm^{-1}, while the bands observed at 3409-3431 cm^{-1} overlap the –OH group. The band observed between 2889-2925 cm^{-1} corresponds to C-H stretching band of PVPCS. A new peak of stretching band is observed at 3430 cm^{-1}, when the PVPCS is added. This broadening suggests that the hydrogen atom take part in intermolecular hydrogen bonding.

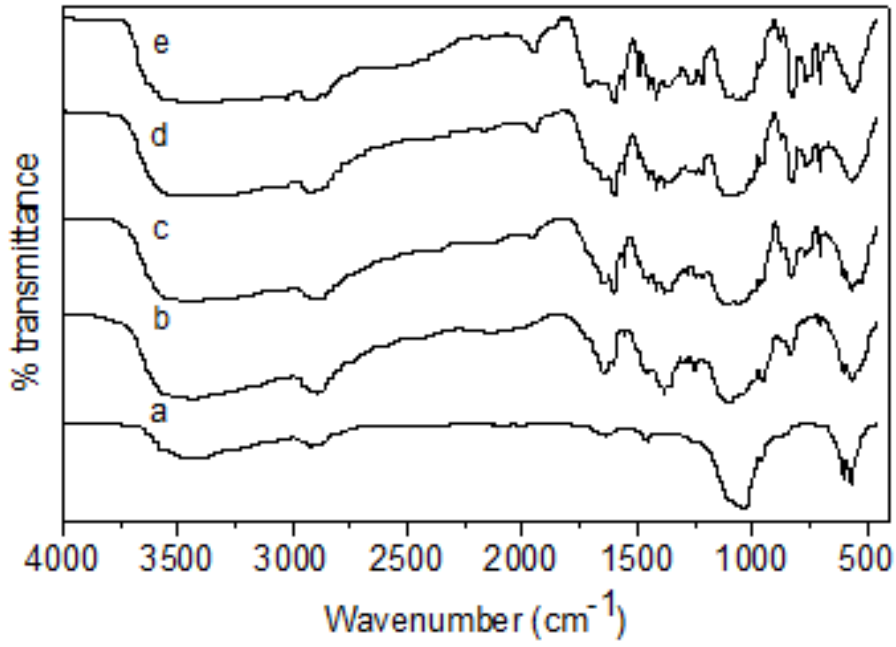

Fig. 2. FTIR Spectrum of (a) nano CHAp, (b) nano CHAp/PVPCS 20, (c) nano CHAp/PVPCS 40, (d) nano CHAp/PVPCS 60 and (e) nano CHAp/PVPCS 80.

Field Emission-Scanning Electron Microscopy. SEM images of pure nano CHAp and different weight percentages of PVPCS compositions are illustrated in Fig. 3. The SEM picture shows that particles exhibit nano rod morphology. The particle size of pure CHAp is 30-80 nm. In case of composites, when the composition of PVPCS is added to CHAp, the rod-like morphology starts to disappear. The increase in the PVPCS compositions i.e., 20, 40, 60 wt. % leads to a corresponding

change from rod-like to an irregular morphology. Further, it is evident that the particle size decreases with increase in PVPCS composition. The elemental analysis (EDAX) of nano PVPCS20/CHAp and nano PVPCS60/CHAp can demonstrate similar composition as illustrated in Fig. 4a. Mineral composition (calcium phosphate: Ca, O, P) and organic content (C) are present in both nanocomposites tested.

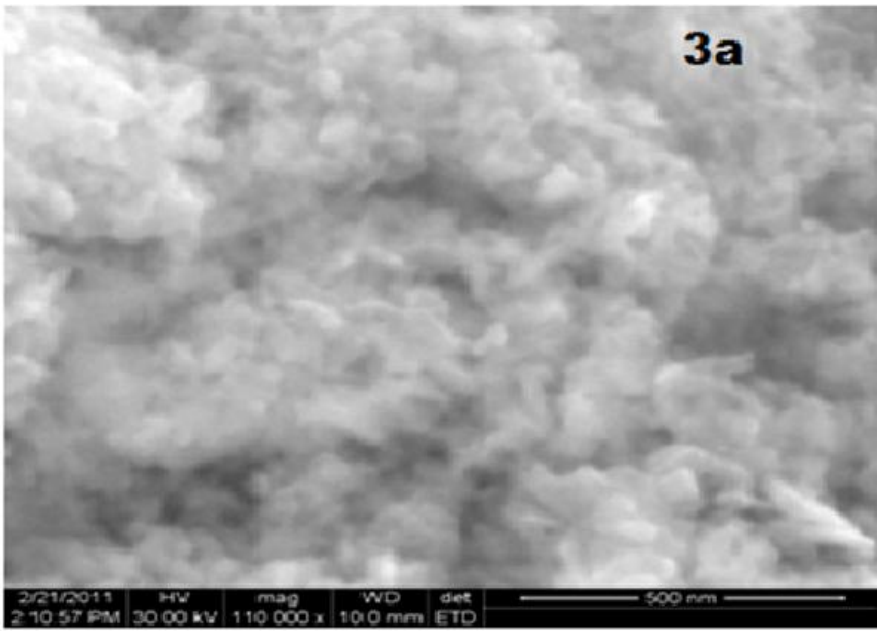

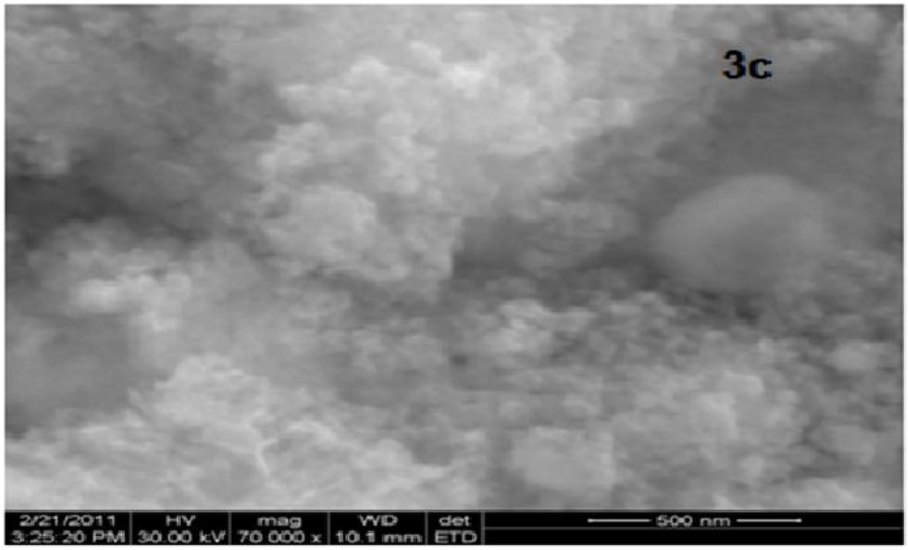

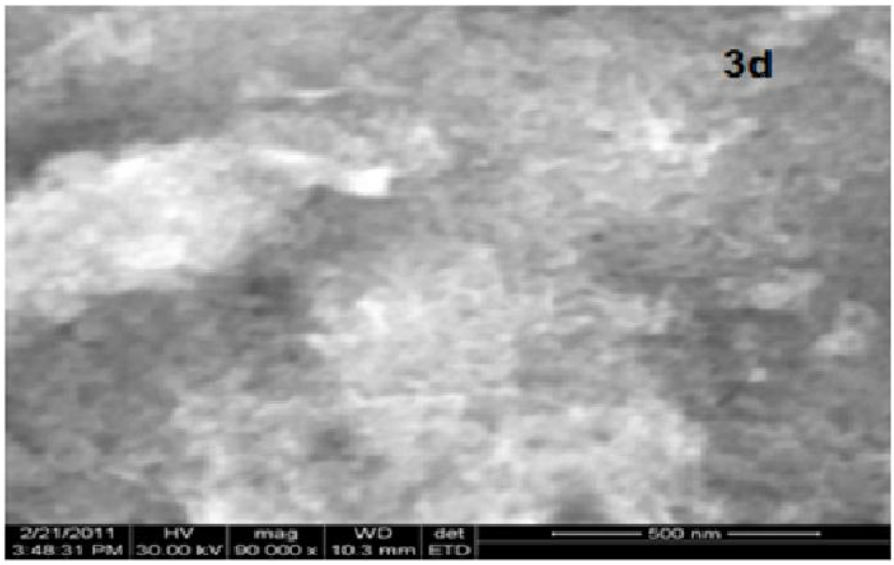

Fig. 3. FE-SEM images of (a) nano CHAp, (b) nano CHAp/PVPCS 20, (c) nano CHAp/PVPCS 40, (d) nano CHAp/PVPCS 60.

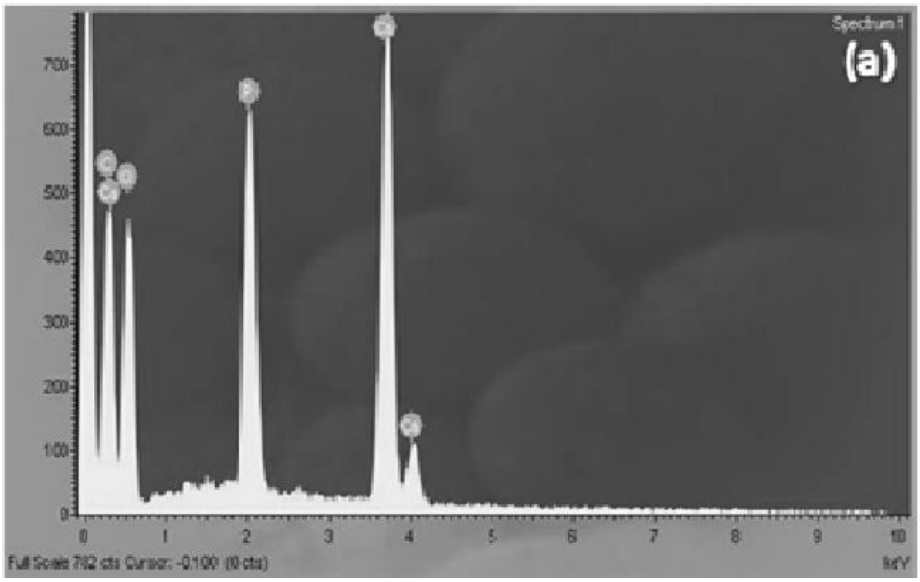

Fig. 4. EDAX Spectrum of (a) nano CHAp/PVPCS 20.

Thermo Gravimetric Analysis. The TGA (Fig. 5) of the PVPCS/CHAp nanocomposites powder was carried out between 50 °C and 1400 °C in air at a heating rate of 20 °C /min. The decomposition behaviour of PVPCS/CHAp nano composite is shown in Fig. 6. The nano CHAp content is calculated from the residual weight in TGA curves at 420 °C. However, since it is very difficult to control adsorbed water content in the composites, this nano CHAp content is only an approximate value. In the TGA curves several steps are observed. The first step, showing a small decrease in weight, is associated with removal of adsorbed moisture, when heated above 120 °C. The second step from 200 to 320 °C mainly due to the dehydration reaction of C-OH groups in PVPCS chains. This temperature shifts to a higher temperature, when the nano CHAp content increases. The third step was degradation of PVPCS matrix releasing CO_2 gas. This temperature shifts to a lower temperature in the TG curves caused by the increasing nano CHAp content. The fact that the second step is initiated at slightly higher temperature and the third step occurs at slightly lower temperature than in pure PVPCS is suggestive of the presence of chemical interaction between PVPCS and the nano CHAp.

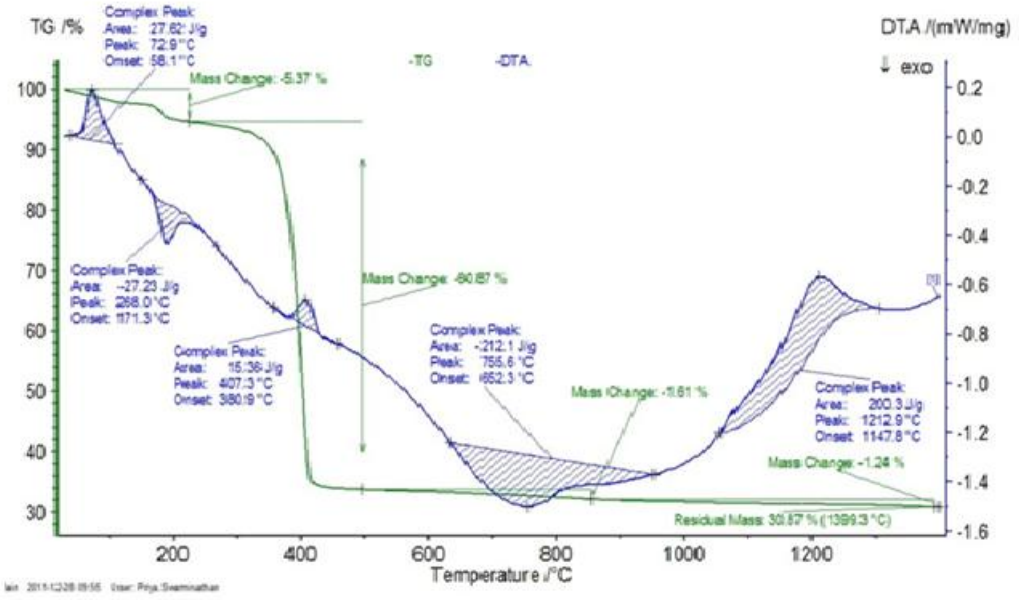

Fig. 5. TGA Curve of nano CHAp/PVPCS 80 Composite

^{31}P MAS-NMR Analysis. The 31P MAS-NMR spectra for the PVPCS/CHAp nanocomposite and nano CHAp powders are shown in Fig. 6. A distinctive resonance peak appears at 2.568 ppm in Fig. 6a for the nano CHAp. After the development of PVPCS/CHAp nano composites, the ^{31}P characteristic peak moves to 2.199 ppm asshown in Fig. 6b, indicating that after the formation nanocomposites, the chemical environment of the phosphorus atom in nano CHAp crystal has been changed. This shift is due to the interaction of CHAp with PVPCS in PVPCS/CHAp nanocomposite. The chemical interaction may be due the hydrogen bonding interaction between the PO_4^{3-} ions of CHAp and the –OH functional groups of PVPCS.

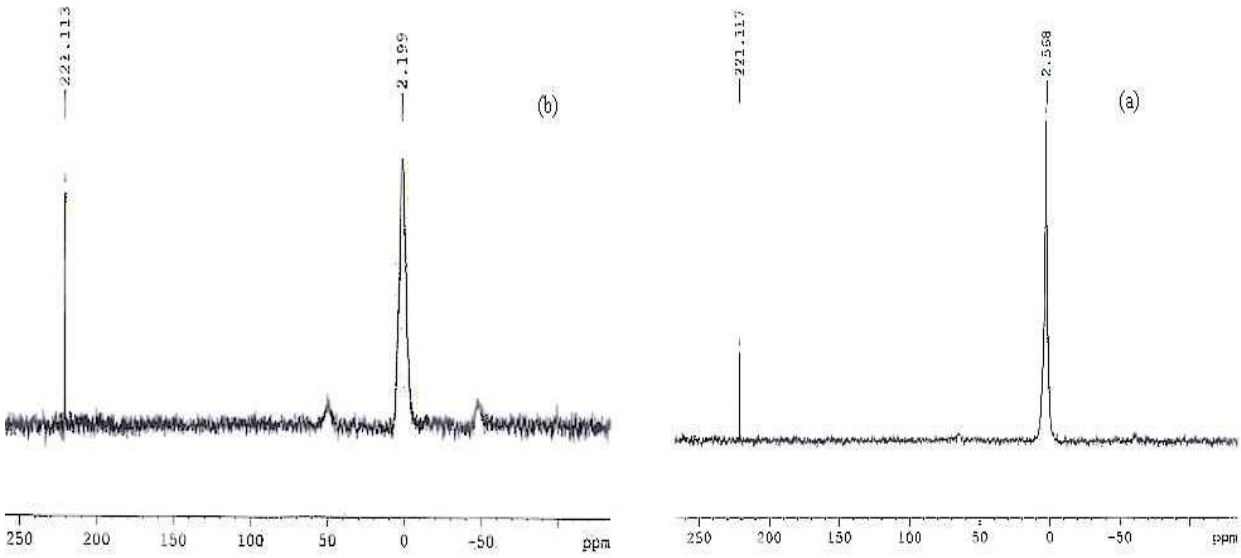

Fig. 6. ^{31}PMAS-NMR Spectra of (a) Nano CHAp and (b) PVPCS40/CHAp nanocomposite

Anti-inflammatory potential analysis. The compound nano CHAp/PVPCS20 and nano CHAp/PVPCS 60 showed significant protection towards HRBC membrane rupture which is induced by hypotonic saline. The effect may be due to the resistance caused by polymers in the destruction of erythrocyte membrane. From the results it was proved that nano CHAp/PVPCS20 composition was more effective than nano CHAp/PVPCS60 composition and also nano CHAp (Table 1). Further work is in progress to identify the exact mechanism involved in anti inflammatory activity [38]. A challenge in regenerative medicine is develop a biomaterial with good mechanical and biological properties and with perspective to act as a cell carrier of stem cells or differentiated cells. Cite at least one article in this area to enhance the relevance of the present study and to discuss future purposes of biomedical applications.

Table 1. Anti-inflammatory activity by HRBC membrane stabilization Method

Concentration in µg/ml	**% inhibition of nano CHAp**	**% inhibition of nano CHAp/PVPCS20 composite**	**% inhibition of nano CHAp/PVPCS60 composite**
1000	92.68	97.16	97.14
800	92.65	98.20	98.12
400	98.57	98.87	98.81
200	98.49	98.86	98.53
100	98.31	98.44	98.40
50	98.27	98.36	98.32
10	99.14	99.22	99.18

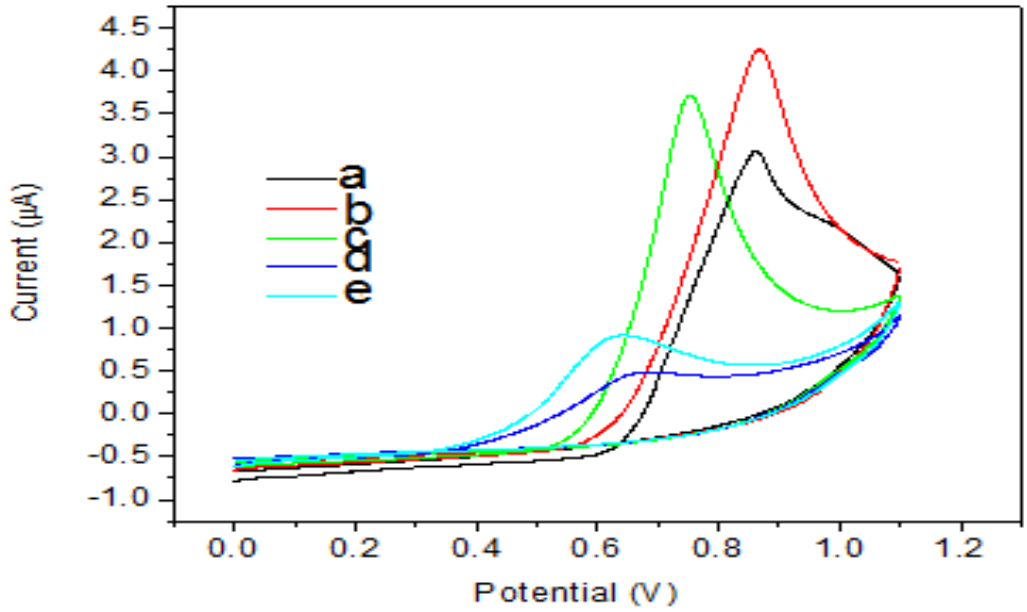

Fig. 7. Cyclic voltammagram images of (a) nano CHAp, (b) nano CHAp/PVPCS 20, (c) nano CHAp/PVPCS 40, (d) nano CHAp/PVPCS 60, (e) nano CHAp/PVPCS 80

Detection of 4-nitro phenol. Fig. 7, shows the electro oxidation of 4-nitro phenol at bare GCE for 1 mM concentration and PVPCS/CHAp nanocomposite modified GCE for 1mM concentration in 0.1 M PBS as the electrolyte. Bare GCE shows a broad oxidation peak at 0.86 V.The modified GCE shows an oxidation peak at 0.62 V with higher current response than the bare GCE (Table 2 and Fig 7). Hence it is clear that the oxidation potential for 4-nitro phenol at the modified electrode was shifted to less positive direction than the bare GCE and the 4-nitro phenol oxidative current was largely increased relative to the bare GCE, indicating the electrochemical detection ability of the PVPCS/CHAp nanocomposite modified electrode. The electro chemical detection of pollutant 4-nitro phenol(4-NP) was carried out by coating the CHAp/PVPCS nanocomposite onto the glassy carbon electrode(GCE) by drop coatingmethod. The electrocatalytic performance of the modified GCE electrode was found to be the best with 4-nitro phenol.

Table 2. Electrochemical oxidation potential value of CHAp/PVPCS nano composite

S.No	Material	Potential(V)
1.	CHAp	0.86
2.	CHAp-PVPCS20	0.86
3.	CHAp-PVPCS40	0.75
4.	CHAp-PVPCS60	0.65
5.	CHAp-PVPCS80	0.62

Conclusions

In the present work, a novel nano CHAp/PVPCS nanocomposite is prepared by simple chemical route. The reduction in particle size with increase in concentration of PVPCS is due to the size control effect of PVPCS molecular structure. The rod-like morphology becomes as an irregular morphology with increase in PVPCS additives. It is inferred that the composition of PVPCS shows significant influence on particle size, thermal stability and antimicrobial activities which facilitate to optimize the composition of composite for particular applications. Nanomaterials are greatly promising in the development of more valuable orthopedic and dental implants. However, the mechanism of interaction between nano CHAp/PVPCS and biologic systems should be investigate thoroughly in future and applied studies using in vitro, in vivo and preclinical methodologies to validate its use for biomedical applications.

Acknowledgement

The authors are grateful for the financial supports from the University Grants Commission and Council of Scientific and Industrial Research, New Delhi, India. The authors are grateful to Metha College of Pharmacy,Thurai pakkam, Chennai, Ramachandra University,Chennai,Tamil Nadu, India.

References

[1] M. Li, X. Xiao, R. Liu, C. Chen, L. Huang, Structural characterization of zinc-substituted hydroxyapatite prepared byhydrothermal method, J. Mater. Sci. Mater. Med. 19 (2008) 797-803.

[2] S. Bose, K.S. Saha, Synthesis and characterization of hydroxyapatite nanopowders by emulsion technique, Chem. Mater. 15 (2003) 4464-4469.

[3] Y. Ding, J. Liu, H. Wang, G. Shen, R. Yu, A piezoelectric immunosensor for the detection of α-fetoprotein using an interface of gold/hydroxyapatite hybrid nanomaterial, Biomaterials 28 (2007) 2147-2154.

[4] H. Wang, Y. Li, Y. Zuo, J. Li, S. Ma, L. Cheng, Biocompatibility and osteogenesis of biomimetic nanohydroxyapatite/polyamide composite scaffolds for bone tissue engineering, Biomaterials 28 (2007) 3338-3348.

[5] V.S. Komlev, S.M. Barinov, F. Rustichelli, Strength enhancement of porous hydroxyapatite ceramics by polymer impregnation, J. Mater. Sci. Lett. 22 (2003)1215-1217.

[6] N. Meenakshi Sundaram, E.K. Girija, M. Ashok, T.K. Anee, R. Vani, R. Suganthi, Crystallisation of hydroxyapatite nanocrystals under magnetic field, Mater. Lett. 60 (2006) 761-765.

[7] V. Rajendran, A. Nishara Begum, M.A. Azooz, F.H. EI Bata, Microstructural dependence on relevant physical–mechanical properties on SiO_2–Na_2O–CaO–P_2O_5 biological glasses, Biomaterials 23 (2002) 4263-4275.

[8] E.S. Ahn, N.J. Gleason, A. Nakahira, J.Y. Ying, Nanostructure processing of hydroxyapatite-based bioceramics, Nano Lett. 1(3) (2001) 149-153.

[9] M. K. Singh, T. Shokuhfar, J. J.D. Almeida Gracio, A. C. M. D. Sousa, J. M. D. F. Fereira, H. Garmestani, S. Ahzi, Hydroxyapatite modified with carbon-nanotube-reinforced poly(methyl methacrylate): A nanocomposite material for biomedical applications, Adv. Funct. Mater. 18 (2008) 694-700.

[10] R. Joseph, K.E. Tanner, Effect of morphological features and surface area of hydroxyapatite on the fatigue behavior of hydroxyapatite-polyethylene composites, Biomacromolecules 6 (2005) 1021-1026.

[11] J.M. Yang, C.S. Lu, Y.G. Hsu, C.H. Shih, Mechanical properties of acrylic bone cement containing PMMA-SiO_2 hybrid solgel material, J. Biomed. Mater. Res. 38 (1997) 143-154.

[12] N. Pramanik, P. Bhargava, S. Alam, P. Pramanik , Processing and properties of nano-and macro-hydroxyapatite/poly (ethyleneco-acrylic acid) composites, Polym. Compos. 27 (2006) 633-641.

[13] M. Boissie`re, P.J. Meadows, R. Brayner, C. Helary, J. Livage, T. Coradin , Turning biopolymer particles into hybrid capsules:the example of silica/alginate nanocomposites, J. Mater. Chem. 16 (2006) 1178-1182.

[14] K. Kawagoe, M. Saito, T. Shibuya, T. Nakashima, K. Hino, H. Yoshikawa, Augmentation of cancellous screw fixation with hydroxyapatite composite resin (CAP) *in vivo,* J. Biomed. Mater. Res. 53 (2000) 678-684.

[15] J. Li, Y. Zuo, X. Cheng, W. Yang, H. Wang, Y. Li, Preparation and characterization of nano-hydroxyapatite/polyamide 66 composite GBR membrane with asymmetric porous structure, J. Mater. Sci, Mater. Med. 20 (2009) 1031-1038.

[16] M. Darder, M. Lo´pez-Blanco, P. Aranda, A. J. Aznar, J. Bravo, E. Ruiz-Hitzky, Preparation and characterization of nano-hydroxyapatite/polyamide 66 composite GBR membrane with asymmetric porous structure, Chem. Mater. 18 (2006) 1602-1610.

[17] Y. Zhang, J. L. A. Mild, Efficient biomimetic synthesis of rodlike hydroxyapatite particles with a high aspect ratio using polyvinylpyrrolidone as capping agent, Cryst. Growth Des. 8 (2008) 2101-2107.

[18] D.Z. Chen, C.Y. Tang, K.C. Chan, C.P. Tsui, P.H.F. Yu, M.C.P. Leung, P.S. Uskokovic, Dynamic mechanical properties and in vitro bioactivity of PHBHV/HA nanocomposite, Compos. Sci. Technol, 67 (2007) 1617-1626.

[19] F.E. Wiria, C.K. Chua, K.F. Leong, Z.Y. Quah, M. Chandrasekaran, M.W. Lee, . Improved biocomposite development of poly (vinyl alcohol) and hydroxyapatite for tissue engineering scaffold fabrication using selective laser sintering, J. Mater. Sci: Mater. Med. 19 (2008) 989-996.

[20] Y. Pan, D. Xiong, Friction properties of nano-hydroxyapatite reinforced poly(vinyl alcohol) gel composites as an articular cartilage, Wear 266 (2009) 699-703.

[21] M. Wang, Y. Li, J. Wu, F. Xu, Y. Zuo, J.A. Jansen, In vitro and in vivo study to the biocompatibility and biodegradation of hydroxyapatite/poly(vinyl alcohol)/gelatin composite, J. Biomed. Mater. Res. Part A 85 (2008) 418-426.

[22] T. Kokubo, H. Takadama, How useful is SBF in predicting in vivo bone bioactivity, Biomaterials, 27 (2006) 2907-2915.

[23] C.W. Chen, C.S. Oakes, K. Byrappa, R.E. Riman, K. Brown, K.S. TenHuisen, V.F. Janas, Synthesis, characterization, and dispersion properties of hydroxyapatite prepared by mechanochemical–hydrothermal methods, J. Mater. Chem. 14 (2004) 2425-2432.

[24] S. Kannan, A.F. Lemos, Synthesis and mechanical performance of biological-like hydroxyapatite, Chem Mater. 18 (2006) 2181-2186.

[25] N. Degirmenbasi, D. M. Kalyon, E. Birinci, Biocomposites of nanohydroxyapatite with collagen and poly (vinyl alcohol), Colloids Surf. B: Biointer. 48 (2006) 42-49.

[26] A. Lak, M. Mazloumi, M. Mohajerani, A. Kajbafvala, S. Zanganeh, H. Arami, S.K. Sadrnezhaad, Self-assembly of dandelionlike hydroxyapatite nanostructures via hydrothermal method, J. Am. Ceram. Soc. 91 (2008) 3292-3297.

[27] L. Yanbao, L. Dongxu, W. Weng, Preparation of nano carbonate-substituted hydroxyapatite from an amorphous precursor, Int.J. Appl. Ceram. Technol. 5 (2008) 442-448.

[28] M.G. Ma, Y. J. Zhu, J. Chang, Monetite formed in mixed solvents of water and ethylene glycol and its transformation to hydroxyapatite, J. Phys. Chem. B. 110 (2006) 14226-14230.

[29] W. Zhang, S.S. Liao, F.Z. Cui, Hierarchical self-assembly of nano-fibrils in mineralized collagen, Chem. Mater, Chem. Mater. 15 (2003) 3221-3226.

[30] L. Bertinetti, A. Tampieri, E. Landi, C. Ducati, P.A. Midgley, S. Coluccia, G. Martra, Surface structure, hydration and cationic sites of nanohydroxyapatite: UHR-TEM, IR, Microgravimetric studies, J. Phys. Chem. C. 111 (2007) 4027-4035.

[31] D. Choi, P.N. Kumta, An alternative chemical route for the synthesis and thermal stability of chemically enriched hydroxyapatite, J. Am. Ceram. Soc. 89 (2006) 444-449.

[32] I.S. Neira, Y.V. Kolen'ko, O.I. Lebedev, G.V. Tendeloo, H.S. Gupta, F. Guitian, M. Yoshimura, An effective Morphology control of hydroxyapatite crystals via hydrothermal synthesis, Cryst. Growth Des, 9 (2009) 466-474.

[33] S. Kannan, J.M.F. Ferreira, Synthesis and thermal stability of hydroxyapatite-β- tricalcium phosphate composites with cosubstituted sodium, magnesium, and fluorine, Chem. Mater. 18 (2006) 198-203.

[34] F. Huang, Y. Shen, A. Xie, J. Zhu, C. Zhang, S. Li, J. Zhu, Study on synthesis and properties of hydroxyapatite nanorods and its complex containing biopolymer, J. Mater. Sci. 42 (2007) 8599 -8605.

[35] R. Murugan, S. Ramakrishna, Bioresorbable composite bone paste using polysaccharide based nano hydroxyapatite, Biomaterials 25 (2004) 3829-3835.

[36] N. Pramanik, S. Mohapatra, S. Alam, P. Pramanik, Synthesis of hydroxyapatite/poly(vinyl alcohol phosphate) nanocomposite and its characterisation, Polym. Compos. 29 (2008) 429-436.

[37] J. Zhan,Y.H. Tseng, C.C. Jerry, Chan, C.Y. Mou, Biomimetic formation of hydroxyapatite nanorods by a single-crystal-to-single-crystal transformation, Adv. Funct. Mater.15 (2005) 2005-2010.

[38] R. Gandhidasan, A. Thamaraichelvan, S. Baburaj, Anti inflammatory action of Lannea coromandelica by HRBC membrane stabilization, Fitoterapia, LXII. 1(1991) 81-83.